Rapid Electrochemical Impedance Spectra Fitting for Lithium-ion Batteries using Geometric-Hybrid Equivalent Circuit Model

Amornthep Sing-se
Advanced Mobility and Propulsion Research Laboratory, Faculty of Engineering, Thai-Nichi Institute of Technology
Bangkok, Thailand
si.amornthep_st@tni.ac.th

Titirat Vivithkeyoonvong
Advanced Mobility and Propulsion Research Laboratory, Faculty of Engineering, Thai-Nichi Institute of Technology
Bangkok, Thailand
titirat@tni.ac.th

Wisit Songmuang
Advanced Mobility and Propulsion Research Laboratory, Faculty of Engineering, Thai-Nichi Institute of Technology
Bangkok, Thailand
wisit@tni.ac.th

Siwalee Choilek
Graduate School of Information Sciences+, Tohoku University
Sendai, Japan
choilek.siwalee.a5@tohoku.ac.jp

Pongkorn Meelapchotipong
Graduate School of Engineering, Tohoku University
Sendai, Japan
meelapchotipong.pongkorn.p1@dc.tohoku.ac.jp

Mahunnop Fakkao
Advanced Mobility and Propulsion Research Laboratory, Faculty of Engineering, Thai-Nichi Institute of Technology
Bangkok, Thailand
*Corresponding author: mahunnop@tni.ac.th

***Abstract*— Electrochemical Impedance Spectroscopy (EIS) is a powerful, non-destructive technique for characterizing lithium-ion batteries. Yet its use in real-time automotive Battery Management Systems (BMS) is limited due to the heavy computational load of traditional complex nonlinear least-squares (CNLS) fitting. In this study, we introduce a rapid hybrid approach that combines geometric and analytical methods to identify the parameters of a commercial Li (Ni, Mn, Co) O_2 pouch cell. By algebraically fitting mid-frequency impedance spectra with circular and rotated-elliptical shapes, the spatial data directly inform initial physical Equivalent Circuit Model (ECM) parameters. This geometry-based initialization avoids the slow iterative optimization bottlenecks. Experimental validations demonstrate that, although the hybrid method slightly reduces diagnostic accuracy—with an average Root Mean Square Error (RMSE) of 0.56% for circles and 0.58% for ellipses, compared to 0.50% with traditional methods—it greatly speeds up processing. Processing times dropped from a fluctuating range of 70.99–194.92 seconds to a steady 7.34–30.77 seconds with the circular hybrid approach. Therefore, this geometry-driven method holds great promise for real-time state estimation on low-power hardware in future electric vehicles.**

***Keywords*— Lithium-ion Battery, Electrochemical Impedance Spectroscopy, Equivalent Circuit Model, Geometric Analysis, State Estimation**

I. INTRODUCTION

The transition towards battery-electric vehicles is driven by their advantages in energy density and well-to-wheel zero-emission performance. Despite these benefits, challenges such as range anxiety, long charging times, and performance uncertainty under dynamic loads persist. To mitigate these issues, the Battery Management System (BMS) must provide precise state estimation, particularly for State-of-Charge (SoC) and State-of-Health (SoH) during operation [1, 2]. Achieving this precision is complicated by the inherent, given the heterogeneity of internal battery dynamics. Advanced *operando* studies using 2D X-ray absorption spectroscopy (2D-XAS) and Computed Tomography XAS have explicitly visualized how charge and discharge reactions proceed in a highly non-uniform manner across composite electrodes, driven by localized microstructural constraints [3-5]. While these high-resolution synchrotron techniques provide invaluable mechanistic insights into cell degradation, they are fundamentally impractical for real-time, on-board vehicle diagnostics. Consequently, a practical BMS must infer these complex, spatially distributed internal states from macroscopic terminal measurements.

Among state estimation methods, electrochemical impedance spectroscopy is a non-destructive frequency-domain technique that characterizes the dynamic behavior of battery electrochemistry, offering insights beyond traditional voltage-current measurements. The impedance response of lithium-ion batteries, often shown in Nyquist plots, describes electrochemical phenomena such as charge-transfer resistance, double-layer capacitance, and Li-ion diffusion processes using equivalent circuit models (ECMs) [3, 4], as shown in Fig. 1.

Conventional methods for extracting ECM parameters from impedance spectra rely on nonlinear optimization algorithms like Nonlinear Least Squares, which, while accurate, are computationally intensive, sensitive to initial guesses, and prone to local minima [6, 7]. Metaheuristic algorithms such as Particle Swarm Optimization, Genetic Algorithm, and Gaining-Sharing Knowledge can avoid local minima by navigating complex landscapes but require more function evaluations [8, 9], limiting their use in real-time BMS diagnostics. Recent automated pipelines combining initial-guess estimation help streamline this process [10]. Empirical ECMs often rely on idealized assumptions, which can lead to overfitting or misrepresentation, especially in heterogeneous systems. Advances include semi-empirical models that

simulate time-domain responses for mechanistic insights [11], but they are computationally intensive for on-board use. The DRT method offers a model-free alternative that decomposes overlapping electrochemical processes into separate peaks [12]. However, classical DRT is an ill-conditioned inverse problem requiring regularization, making it more computationally demanding than traditional fitting methods.

Recently, geometric analysis has become a quick and focused method for parameterizing -R//CPE- (resistor-constant phase element parallel) configurations [13]. In actual battery systems, surface heterogeneity and variable reaction rates cause ideal semicircles to appear as depressed semicircles or squashed elliptical arcs in Nyquist plots [6, 14]. By fitting circles or ellipses directly to these specific frequency ranges, geometric techniques can determine model parameters algebraically from the arc's center, radius, and depression angle. This purely geometric method avoids iterative optimization procedures, significantly reducing computational effort and eliminating concerns about sensitivity to initialization [13].

Despite its computational advantages, critical research gaps prevent the widespread adoption of geometric fitting for commercial cells, such as Nickel-Manganese-Cobalt (NMC) chemistries. Previous geometric-based ECM fitting research has primarily focused on parameterizing simple depressed semicircles and has noted a distinct lack of advanced composite geometric frameworks capable of separating merged arcs. When multiple electrochemical processes overlap significantly in the frequency domain, simple geometric models merge them into composite shapes, leading to misattributed impedance contributions [1-2, 7].

Therefore, the objective of this work is to introduce a novel, rapid ECM-fitting framework that goes beyond simple semicircles. By combining both circles and rotated ellipses, this composite advanced geometric analysis effectively decomposes the overlapping impedance spectra typical of commercial batteries

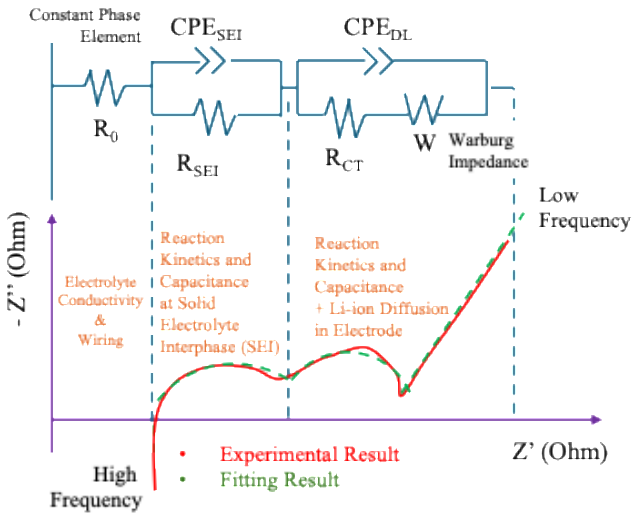

Fig. 1. Equivalent circuit model fitting for Li-ion batteries.

II. Methodology

A. Experimental Setup

A commercially available pouch cell battery with an NMC composite cathode and a graphite anode, with a capacity of 3 Ah, was used. The model battery was electrochemically controlled using a Potentio/Galvanostat (BioLogic VSP-3e). During the charging test, a constant current of 1 A was applied to the model battery with a cut-off voltage of 4.2 V. Electrochemical impedance spectroscopy (EIS) was performed intermittently over the frequency range from 10 kHz to 10 mHz. A small amplitude of 10 mV was applied at each 1% SoC increment to measure the impedance spectra.

Computational analyses, including ECM fitting and conventional nonlinear least-squares benchmarking, were carried out on a laptop equipped with an Intel Core i7-13620H and 16 GB of RAM, using Python.

B. Data Integrity and Validation

Before extracting parameters, the raw experimental EIS data were subjected to a Linear Kramers-Kronig (Lin-KK) validity test. The Kramers-Kronig relations are fundamental mathematical principles that relate the real and imaginary parts of a complex impedance response, provided the system is linear, causal, and stable.

Rather than directly solving complex, highly sensitive integral equations, the Lin-KK approach assesses compliance by fitting experimental data to a generalized measurement model that is inherently KK-compliant. This model typically includes an ohmic resistance (R_0), a series inductance (L_0), and a capacitor impedance ($Z_{KK}(\omega)$) defined as (1).

$$Z_{KK}(\omega) = j\omega L_0 + R_0 + \sum_{k=1}^{M} \frac{R_k}{1 + j\omega\tau_k} \quad (1)$$

where τ_k represents an array of fixed time constants distributed logarithmically across the measured frequency range, and R_k are the resistance values optimized during the fitting process.

Once the optimal KK-compliant model is constructed, the algorithm calculates the fractional residual errors between the experimental measurements (Z_{exp}) and the idealized Lin-KK spectra (Z_{KK}). The residuals for the real (Δ_{RE}) and imaginary (Δ_{IM}) components are normalized by the absolute magnitude of the experimental impedance at each frequency point as expressed in (2) and (3), respectively.

$$\Delta_{RE}(\omega) = \frac{Z'_{exp}(\omega) - Z'_{KK}(\omega)}{|Z_{exp}(\omega)|} \times 100\% \quad (2)$$

$$\Delta_{IM}(\omega) = \frac{Z''_{exp}(\omega) - Z''_{KK}(\omega)}{|Z_{exp}(\omega)|} \times 100\% \quad (3)$$

These residuals provide a highly sensitive quantitative method for identifying measurement artifacts. If the maximum absolute residual error in either the real or imaginary part exceeded 1.0%, the impedance spectra were deemed to deviate from linearity. While rigorous laboratory measurements often target residuals below 0.5%, the 1.0% threshold was explicitly chosen to accommodate the inherent noise and slight nonlinearities typical of commercial pouch

cells operating over a wide SoC range. Crucially, this slightly relaxed threshold was also necessary to maintain a robust, continuous dataset of valid spectra under intermittent measurement conditions, preventing excessive data loss that would disrupt the SoC-dependent analysis. Visual inspection of the residual plots versus frequency confirmed that the errors within the accepted spectra were randomly distributed, indicating standard measurement noise rather than systematic model inadequacy or structured drift. Spectra exhibiting clear systematic frequency-dependent trends were excluded from the dataset. In this experiment, no EIS spectra were excluded based on this criterion.

C. Equivalent Circuit Model Fitting

In this work, the characteristics of the lithium-ion battery are analyzed using a modified ECM, specifically the modified Randles circuit model shown in Fig. 1. The ECM includes an initial series inductor (L_0) and an ohmic resistance (R_0), followed by two parallel networks. The first network (R_{SEI}//CPE_{SEI}) captures the reaction kinetics and capacitance of the solid electrolyte interphase (SEI) at mid frequencies. The second network models low-frequency diffusion processes within the electrode, consisting of a charge-transfer resistance (R_{CT}) in series with a Warburg impedance (Z_W), both in parallel with a second constant phase element that represents the double-layer capacitance of the porous electrode (CPE_{dl}). The overall impedance ($Z_{total}(\omega)$) is given by (4).

$$Z_{total}(\omega) = j\omega L_0 + R_0 + \left[\frac{1}{R_{SEI}} + Q_{SEI}(j\omega)^{n_{SEI}}\right]^{-1} + \left[\left(R_{CT} + Z_W(\omega)\right)^{-1} + Q_{dl}(j\omega)^{n_{dl}}\right]^{-1} \quad (4)$$

where Q_{SEI} and Q_{dl} are the CPE coefficients of solid electrolyte interphase, and double layer capacitor, respectively, ω is the angular frequency, and n_{SEI}, *and* n_{dl} are the fractional exponents of each CPE element ($0 \leq n \leq 1$) that represent the degree of surface heterogeneity of solid electrolyte interphase, and composite electrode, respectively.

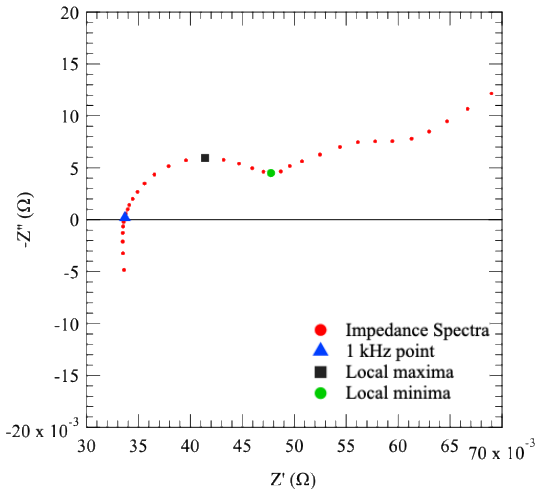

Fig. 2. The three key points of detection for geometric analysis.

D. Geometric Fitting Techniques

To alleviate the computational load of iterative optimization, this work proposes a hybrid geometric-to-analytical fitting framework that extracts ECM parameters from the impedance spectra.

1) Impedance spectra segmentation

To prevent high-frequency noise from affecting the geometric extraction, a Savitzky-Golay (SG) filter employs cubic polynomial regression to smooth the imaginary parts of the impedance spectra. This filter preserves the height and shape of the Nyquist arc, ensuring the true local maximum is accurately identified without distortion. Once the characteristic peak frequency (f_{peak}) is determined, the algorithm segments the mid-frequency arc by dynamically locating the high-frequency onset point and the subsequent low-frequency local minimum, which marks the transition into the diffusion tail. Fig. 2 shows an example with three key points, *i.e.*, the high-frequency onset near 1 kHz (blue triangle), the local maximum (black square), and the subsequent local minimum in the valley indicating the shift into the low-frequency diffusion tail (green dot). Using these point coordinates, the algorithm fits geometric primitives algebraically rather than iteratively.

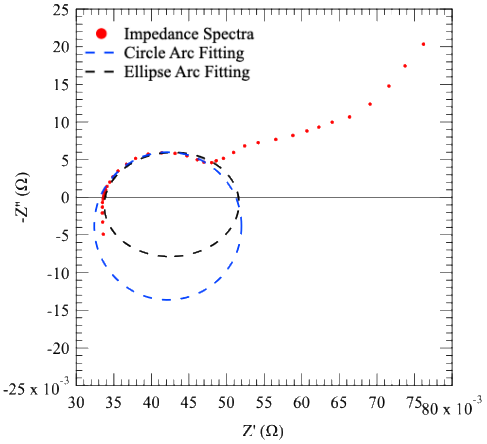

Fig. 3. Circle and ellipse arc fitting on impedance spectra.

2) Algebraic Circle Fitting with Adaptive Weighting

For impedance arcs that closely resemble depressed semicircles, the algorithm uses a weighted algebraic least-squares fit. The general equations for a circle and linear polynomial form are given as (5) and (6), respectively.

$$(x - x_c)^2 + (y - y_c)^2 = R_{arc}^2 \quad (5)$$

$$Ax + By + C = -(x^2 + y^2) \quad (6)$$

Where x_c, y_c represent the center coordinate of circle.

To solve the circle equation, a design matrix $\boldsymbol{M} = [x, y, 1]$ and dependent variable vector $\boldsymbol{b} = -(x^2 + y^2)$ are created to determine the parameter vector $\boldsymbol{p} = [A, B, C]$. To accurately capture the crest of the impedance arc, the algorithm uses an adaptive weighting scheme. The weights are proportional to the squared magnitude of the normalized imaginary impedance, as defined in (7), with a minimum threshold set at 0.05 to prevent low-frequency tails from dominating the solution. These parameters are determined by minimizing the weight cost function described in (8).

$$w = \left(\frac{|y|}{y_{max}}\right)^2 \quad (7)$$

$$cost = min\left|\left|W \cdot (M \cdot p - b)\right|\right|^2 \quad (8)$$

A physical constraint mandates that the arc's center be below the real axis for accurate modeling of CPE behavior, illustrated by the black circle in Fig. 3. If the algebraic solution suggests it above, a bounded least-squares optimization prevents it from leaving the physically valid domain.

3) Elliptical Arc Fitting via Eigenvalue Formation

In real battery systems, surface heterogeneity and variable reaction rates cause ideal semicircles to appear as depressed semicircles or squashed elliptical arcs. A standard CPE effectively models a symmetric distribution of relaxation times. However, when SEI and charge-transfer processes overlap in highly heterogeneous composite electrodes, they yield asymmetric distributions. The rotated ellipse empirically captures this asymmetry; its eccentricity correlates with the width of the merged time constants, while the rotation angle reflects the phase shift between the overlapping interfacial phenomena. This allows the algorithm to mathematically decouple overlapping electrochemical processes.

First, the algorithm normalized the input coordinates by their mean and standard deviation to ensure numerical stability. The ellipse arc was formulated using the general conic (9), subject to the ellipse-specific constraint $4AC\text{-}B^2=1$.

$$Ax^2 + Bxy + Cy^2 + Dx + Ey + F = 0 \quad (9)$$

The data matrices are partitioned into quadratic terms $D_1 = [x^2, xy, y^2]$ and linear term $D_2 = [x, y, 1]$. Subsequently, the total scatter matrix is partitioned into sub-matrices using dot products as $S_1 = D_1^T D_1$, $S_2 = D_1^T D_2$, and $S_3 = D_2^T D_2$. By applying Lagrange multipliers to minimize the algebraic distance subject to the ellipse constraint, the linear terms are analytically eliminated, reducing the system to a generalized eigenvalue problem as expressed in (10)

$$C_1^{-1}(S_1 - S_2 S_3^{-1} S_2^T)\boldsymbol{a_1} = \lambda \boldsymbol{a_1} \quad (10)$$

Where $\boldsymbol{a_1} = [A, B, C]^T$. The eigenvector corresponding to the single positive eigenvalue (λ) yields the optimal quadratic coefficients, from which the linear parameters and the ellipse's geometric properties—center coordinates (x_c, y_c), semi-major axis (a), semi-minor axis (b), and rotation angle (θ)—are explicitly derived as illustrated in the blue ellipse of Fig. 3.

4) ECM Parameters Conversion

Once the optimal circle or ellipse fits the mid-frequency arc, its spatial features are mathematically converted into the ECM parameter of the R_{SEI}//CPE_{SEI} branch, avoiding nonlinear solvers. The charge-transfer resistance (R_{SEI}), indicating kinetic resistance at the electrode-electrolyte interface, equals the real-axis horizontal span of the arc: as the diameter (2R) for circles, or from maximum horizontal span (2a) for ellipses after un-rotating dataset. The CPE fractional exponent (n_{CPE}), which indicates non-ideal distributed capacitance, is derived from the depression angle (θ_{dep}) of circular arcs using (11).

$$n_1 = 1 - \left(\frac{2\theta_{dep}}{\pi}\right) \quad (11)$$

For highly distorted elliptical arcs, this non-ideality is approximated using the elliptical aspect ratio (b/a), bounded between 0.41 and 0.99. The CPE coefficient at solid-electrolyte interphase (Q_{SEI}) is then determined algebraically from the characteristic peak frequency during Savitzky-Golay segmentation, resulting in the closed-form solution in (12).

$$Q_{SEI} = \frac{1}{R_{CPE}\left(2\pi f_{peak}\right)^{n_{CPE}}} \quad (12)$$

Applying these algebraic translations produces an accurate, physically based parameter set for the mid-frequency reactions. It is noted that the geometric conversion yields closed-form solutions only for high- to mid-frequency components. Because the low-frequency Warburg impedance does not have a closed-form expression, its parameters cannot be derived algebraically. Instead, the extracted mid-frequency geometric parameters are used as initial bounds for the global optimization solver. By isolating the high- and mid-frequency parameters, this hybrid approach drastically reduces degrees of freedom and mitigates the identifiability problems typically associated with overlapping arcs, allowing the solver to efficiently address the remaining low-frequency diffusion components.

E. Model Validation

To validate the accuracy of the proposed geometric fitting algorithm and benchmark its parameter settings against conventional optimization techniques, a least-squares objective function was used. This function serves as the standard metric by evaluating the deviation between EIS measurements and ECM theoretical predictions. The sum of squared errors, evaluated over the full frequency spectrum, is given by (13).

$$S(\theta) = \sum_{i=1}^{N}\left[\left(Z'_{exp}(\omega_i) - Z'_{model}(\omega_i,\theta)\right)^2 + \left(Z''_{exp}(\omega_i) - Z''_{model}(\omega_i,\theta)\right)^2\right] \quad (13)$$

where $Z'_{exp}(\omega_i)$ and $Z''_{exp}(\omega_i)$ represent real and imaginary impedance value obtained from the measured impedance spectra at the frequency point i, respectively. $Z'_{model}(\omega_i,\theta)$ and $Z''_{model}(\omega_i,\theta)$ are the real and imaginary impedance predicted by the ECM equation. The variable N denotes the total number of frequency points

III. Results and Discussions

Fig. 4 shows the charging profile and the corresponding impedance spectra of the model battery across various SoC. Due to performance uncertainties inherent in randomly selected commercial products, the model cell reached the 4.2 V cut-off voltage at a capacity of 2.45 Ah, which is marginally lower than its claimed nominal capacity. As shown in Fig. 4(a), voltage fluctuations during the testing cycle indicate the programmed transitions between the constant-current charging modes and the open-circuit relaxation periods, which are required for stable EIS measurements. Fig. 4(b) presents the resulting impedance spectra, with the color gradient tracking the SoC evolution, *i.e.*, blue spectra represent lower

charge states beginning at 3.0 V, while red spectra correspond to high charge states approaching the cut-off voltage at 4.2 V.

Figure 5 (a)–(i) demonstrates the outputs of the proposed geometric-hybrid ECM algorithms (circular and elliptical) to parameterize these spectra. The outputs are compared with the conventional unseeded least-squares ECM fitting within specific SoC intervals. Results confirm that both the circle- and ellipse-hybrid ECM algorithms effectively capture the depressed semicircles and accurately follow the experimental impedance trajectories at each tested voltage.

The statistical diagnostic accuracy of these methods across the entire SoC range is shown in Fig. 5(j). The conventional ECM fitting algorithm achieved a baseline Root Mean Square Error (RMSE) of 0.50%, with a 95% confidence interval on the mean of (0.44, 0.55). The proposed geometric methods maintained highly competitive accuracy; the circle-hybrid ECM had an average RMSE of 0.56% with an interval of (0.49, 0.62), while the ellipse-hybrid ECM resulted in an RMSE of 0.58% with an interval of the mean of (0.48, 0.68).

While geometric fitting results in minimal loss of accuracy, its main benefit lies in addressing the significant computational bottlenecks that hinder real-time BMS integration. To assess these efficiency gains, total execution times were measured over the 3.0 V to 4.2 V range. As shown on the logarithmic scale in Fig. 6(a), the conventional optimization-based ECM fitting (blue) displayed high computational variability. At certain voltage points, processing times for the conventional method increased sharply, sometimes exceeding 10^3 s per spectrum. This instability reveals a key flaw in standard unseeded algorithms; their high sensitivity to poor initial guesses, which leads the solver to perform many function evaluations and get trapped in local minima.

In contrast, the geometric hybrid methods effectively avoided these iterative delays. As shown in the distribution plot at the 95% confidence level in Fig. 6(b), the conventional ECM required substantial computation time, ranging from 70.99 to 194.92 s. These extensive baseline times result from the unseeded nature of the conventional standard least-squares algorithm. Without highly accurate initial parameters, the solver struggles with the identifiability of overlapping arcs, forcing it to perform an excessive number of function evaluations to escape local minima.

Using algebraically derived spatial parameters as initial seeds, the circle-hybrid ECM emerged as the most efficient and stable method, drastically cutting down computation times to between 7.34 and 30.77 s. Although the ellipse-hybrid ECM showed more variability, with times ranging from 5.98 to 151.85 s—mainly due to the complex matrix operations needed for the generalized eigenvalue formulation on distorted arcs—it still achieved the fastest processing at its best. While the circle-hybrid ECM is extremely efficient overall, the ellipse-hybrid approach offers a distinct advantage in certain cell conditions. Despite greater computational variability due to complex matrix operations, elliptical fitting performs better for highly degraded batteries or extremely low temperatures, where reaction arcs become highly asymmetric and cannot be accurately modeled by a uniform circular depression.

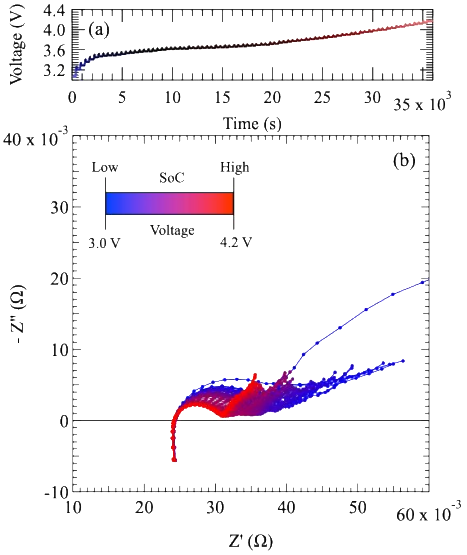

Fig. 4. Electrochemical test result of model battery; (a) charging profile, (b) impedance spectra.

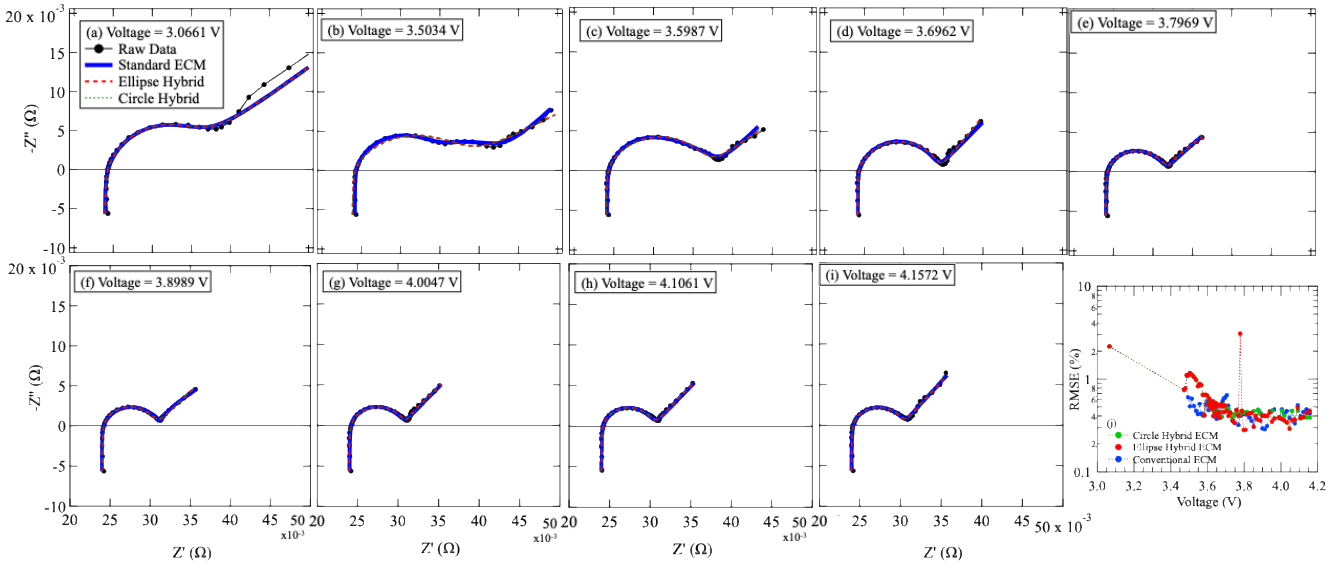

Fig. 5. Comparison between fitting techniques at various charging voltages; (a) Open-circuit voltage at 3.0 V, (b) 3.5 V, (c) 3.59 V, (d) 3.69 V, (e) 3.79 V, (f) 3.89 V, (g) 4.0 V, (h) 4.1 V, (i) Cut-off voltage, (j) Root mean square error for each techniques at specfic voltage.

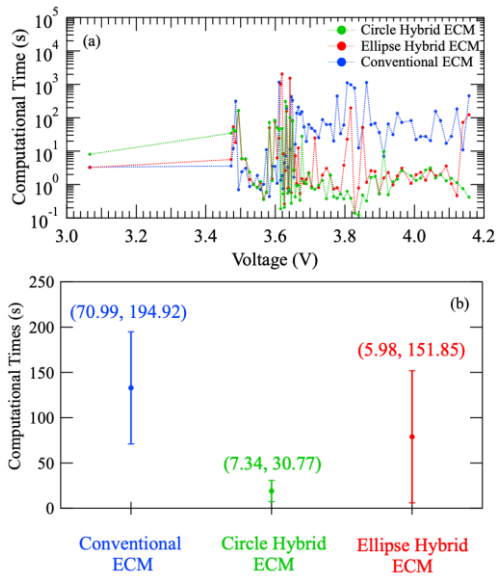

Fig. 6. Computational time comparison between fitting techniques; (a) vary by charging voltage, (b) the 95% confident interval on mean of computational time

These comparative results clearly show that geometry-fitted ECMs effectively steer the solver to the global optimum. They significantly cut down computational time while only slightly reducing fitting accuracy by less than 0.1%. The proposed geometric hybrid framework is therefore very well-suited for incorporation into next-generation, real-time battery management systems.

CONCLUSIONS

This study introduces a rapid geometric-to-analytical hybrid framework to enhance ECM fitting from EIS data in lithium-ion batteries. By extracting spatial features from impedance arcs using circle and ellipse fitting, it converts geometry into initial electrochemical parameters, reducing the computational bottlenecks and local minima commonly seen with CNLS methods. Experimental tests from 3.0 V to 4.2 V showed significant improvements, *i.e.*, processing time per spectrum decreased from 132.95 to 19.06 s for Circle Hybrid ECM and to 78.91 s for Ellipse Hybrid ECM, with minimal loss in accuracy (RMSE from 0.50% to approximately 0.56-0.58%). The framework efficiently and rapidly derives SEI and charge-transfer parameters, making it suitable for advanced Battery Management Systems (BMS). Future research will explore this approach in real-time automotive scenarios, such as low-power embedded microcontrollers.

ACKNOWLEDGMENT

This work is financially supported by the Takahashi Industrial and Economic Foundation in Fiscal Year 2024 and by the Special Endowed Course for Green Industrial Transformation towards Sustainability, funded by the AEM-METI Economic & Industrial Cooperation Committee (AMEICC).

REFERENCES

[1] G. Patrizi, F. Canzanella and L. Ciani, "Towards a Novel Indirect Battery Health Indicator Based on Electrochemical Impedance Spectroscopy for RUL Estimation in Electric Vehicles," in *2025 IEEE International Workshop on Metrology for Automotive (MetroAutomotive)*, Parma, 2025.

[2] S. Yang, C. Zhang, J. Jiang, W. Zhang, L. Zhang and Y. Wang, "Review on state-of-health of lithium-ion batteries: Characterizations, estimations and applications," *Journal of Cleaner Production,* vol. 314, p. 128015, 2021.

[3] T. Nakamura, K. Chiba, M. Fakkao, Y. Kimura, K. Nitta, Y. Terada, Y. Uchimoto and K. Amezawa, "Operando observation of formation and annihilation of inhomogeneous reaction distribution in a composite electrode for lithium ion batteries," *Batteries & Supercaps,* vol. 2, no. 8, pp. 688-694, 2019.

[4] Y. Kimura, A. Tomura, M. Fakkao, T. Nakamura, N. Ishiguru, O. Sekizawa, K. Nitta, T. Uruga, T. Okumura, M. Tada, Y. Uchimoto and K. Amezawa, "3D Operando Imaging and Quantification of Inhomogeneous Electrochemical Reactions in Composite Battery Electrodes," *The Journal of Physical Chemistry Letters,* vol. 11, no. 9, pp. 3629-3636, 2020.

[5] M. Fakkao, K. Chiba, Y. Kimura, T. Nakamura, T. Okumura, K. Nitta, Y. Terada, Y. Uchimoto and K. Amezawa, "Visualization of the reaction distribution in a composite cathode for an all-solid-state lithium-ion battery," *Journal of the Ceramic Society of Japan,* vol. 125, no. 4, pp. 299-302, 2017.

[6] E. Locorotondo, V. Cultrera, L. Pugi, L. Berzi, M. Pasquali and N. Andrenacci, "Impedance spectroscopy characterization of lithium batteries with different ages in second life application," in *2020 IEEE International Conference on Environment and Electrical Engineering and 2020 IEEE Industrial and Commercial Power Systems Europe (EEEIC / I&CPS Europe)*, Madrid, 2020.

[7] Y. Wu and B. Balasingam, "A Comparison of Battery Equivalent Circuit Model Parameter Extraction Approaches Based on Electrochemical Impedance Spectroscopy," *Batteries,* vol. 10, no. 400, pp. 1-25, 2024.

[8] Meddings, Nina; Heinrich, Marco; Overney, Frederic; Lee, Jong-Sook; Ruiz, Vanes; Napolitano, Emilio; Seitz, Steffen; Hinds, Gareth; Raccichini, Rinaldo; Gaberscek, Miran; Park, Juyeon;, "Application of electrochemical impedance spectroscopy to commercial Li-ion cells: A review," *Journal of Power Sources,* vol. 480, p. 228742, 2020.

[9] J.-S. Pan, L.-F. Liu, S.-C. Chu, P.-C. Song and G.-G. Liu, "A New Gaining-Sharing Knowledge Based Algorithm with Parallel Opposition-Based Learning for Internet of Vehicles," *Mathematics,* vol. 11, no. 2953, pp. 1-25, 2023.

[10] Y. Pan, J. Meng, S. Zhang, W. Liu, J. Fu, Q. Peng, B. Xiao and Z. Song, "An automated circuit model for electrochemical impedance spectroscopy explanation of lithium-ion batteries," *Journal of Energy Storage,* vol. 127, p. 117147, 2025.

[11] W. Pholauyphon, J. Aekchat, K. Nantasaksiri, T. Suzuki, S. Tsushima and P. Charoen-amornkitt, "Semi-empirical physics-based simulation of time-domain current responses in electrochemical impedance spectroscopy and their conversion to frequency-domain spectra," *Journal of Energy Storage,* vol. 150, p. 119976, 2026.

[12] L. Wildfeuer, P. Gieler and A. Karger, "Combining the Distribution of Relaxation Times from EIS and Time-Domain Data for Parameterizing Equivalent Circuit Models of Lithium-Ion Batteries," *Batteries,* vol. 7, no. 52, pp. 1-23, 2021.

[13] Z. Zhou, Y. Li, Q.-G. Wang and J. Yu, "Health Indicators Identification of Lithium-Ion Battery From Electrochemical Impedance Spectroscopy Using Geometric Analysis," *IEEE Transactions on Instrumentation and Measurement,* vol. 72, no. 1501709, 2023.

[14] J. Liu, D. Li, Z. Zhang, L. Li, H. Ma and Z. Yu, "A Complex Parameter Circuit Model Based on Impedance Spectrum of Lithium Iron Phosphate Power Battery". China Patent CN206497454U, 15 09 2017.

[15] S. Mosamane, P. Barendse and P. Pillay, "A Novel Technique for Simultaneous EIS Measurements in Solar-Battery Hybrid Systems Using a Boost Converter," in *2025 IEEE Energy Conversion Conference Congress and Exposition (ECCE)*, Philadelphia, 2025.

[16] P. Iurilli, C. Brivio, R. E. Carrillo and V. Wood, "EIS2MOD: A DRT-Based Modeling Framework for Li-Ion Cells," *IEEE Transactions on Industry Applications,* vol. 58, no. 2, pp. 1429 - 1439, 2022.